Deep-Sea Research I 92 (2014) 93–106

Contents lists available at ScienceDirect

Deep-Sea Research I

journal homepage: www.elsevier.com/locate/dsri

Biogeochemical variability in the southern Ross Sea as observed by a glider deployment

Daniel E. Kaufman [a,*], Marjorie A.M. Friedrichs [a], Walker O. Smith Jr.[a], Bastien Y. Queste [b], Karen J. Heywood [b]

[a] Virginia Institute of Marine Science, College of William & Mary, P.O. Box 1346, Gloucester Point, VA 23062, USA
[b] Centre for Ocean and Atmospheric Sciences, School of Environmental Sciences, University of East Anglia, Norwich, NR4 7TJ, UK

ARTICLE INFO

Article history:
Received 16 January 2014
Received in revised form
18 June 2014
Accepted 25 June 2014
Available online 15 July 2014

Keywords:
Ross Sea
Phytoplankton
Glider
Modified Circumpolar Deep Water

ABSTRACT

High-resolution autonomous glider data (including temperature, salinity, fluorescence, and optical backscatter) collected during the 2010–2011 austral summer identified variations in phytoplankton biomass along two glider sections near 76°40′S. Sea surface temperatures were warmer during the latter, westward section, while mixed layer depths were deeper. Substantial quantities of Modified Circumpolar Deep Water, identified by neutral density criteria, were located within both sections. Chlorophyll (Chl) concentrations computed from fluorescence exhibited daily quenching near the surface, and deep chlorophyll concentrations at 200 m became periodically elevated, suggesting substantial export on small space and time scales. The concentrations of particulate organic carbon (POC) computed from backscatter increased abruptly during the latter, westward section, concurrent with a decrease in chlorophyll. These higher POC:Chl ratios were not strongly correlated with presence of MCDW or with shallower mixed layer depths, but were strongly associated with higher surface temperatures and wind speed. The observed POC:Chl increase suggests a marked spatial and temporal transition between a *Phaeocystis antarctica*-dominated assemblage characterized by modest POC:Chl ratios to a diatom-dominated assemblage. Finally, a subsampling analysis highlights the capability of high-resolution glider data to resolve these biological/physical parameter correlations that are not discernible from lower frequency data typical of traditional cruise stations.

1. Introduction

In situ observations and satellite-derived data from the Ross Sea have revealed high phytoplankton biomass and productivity compared with much of the rest of the Southern Ocean (Arrigo et al., 2008; Smith and Comiso, 2008). In addition, these data have demonstrated considerable variability on a suite of time and space scales, yet the mechanisms responsible for this variability are not yet well understood (Peloquin and Smith, 2007). An improved understanding of mesoscale controls on phytoplankton biomass and composition will provide important insights into the dynamics of the Ross Sea food web and reveal how this food web is responding to physical changes that are already occurring, such as freshening (Jacobs et al., 2002; Jacobs and Giulivi, 2010), increases in ice extent (Massom and Stammerjohn, 2010), decreases in ice-free duration of the polynya (Stammerjohn et al., 2012), and wind changes (Bracegirdle et al., 2008).

Previous cruise-based observational programs within the Southern Ross Sea have revealed that two dominant bloom-forming phytoplankton groups, haptophytes and diatoms, commonly occur and show distinct seasonal cycles of growth (Smith et al., 2010) that help support the region's sizeable contribution to the biogeochemical cycles of the Southern Ocean (Arrigo et al., 2008). Phytoplankton growth begins early each austral spring (late October) when the dominant haptophyte, *Phaeocystis antarctica* grows rapidly and reaches maximum biomass in mid- to late-December (Smith et al., 2000). Growth and biomass then decline rapidly (over a few weeks). Although the mechanism for this sudden decline is not well understood, it has been hypothesized to be a result of iron limitation and rapid sedimentation of aggregates (Smith et al., 2000; Arrigo et al., 2003). Elevated chlorophyll concentrations in the euphotic zone have been shown to be associated with rapid (on the order of days) sinking and flux of phytoplankton to depth in summer (Smith et al., 2011b). In contrast to the strong seasonal cycle of *P. antarctica*, diatoms are present at varying concentrations throughout the growing season; however, a late summer secondary bloom has been observed in some years (Peloquin and Smith, 2007; Smith et al., 2011a).

The domains in which these two phytoplankton groups dominate are often spatially distinct and exhibit distinct ratios of

* Corresponding author. Tel.: +1 804 684 7739.
E-mail address: dekaufman@vims.edu (D.E. Kaufman).

http://dx.doi.org/10.1016/j.dsr.2014.06.011

particulate organic carbon (POC) to chlorophyll (Chl). Lower POC: Chl ratios are often associated with *P. antarctica*, and higher ratios are associated with diatoms during late summer (DiTullio and Smith, 1996; Smith et al., 2000). *Phaeocystis antarctica*, which exists in both solitary and colonial forms (Schoemann et al., 2005), typically dominates in the central Ross Sea polynya where there are relatively deep mixed layers (Arrigo et al., 1998; Smith et al., 2010); conversely, diatoms dominate in regions with shallow mixed layers, such as near retreating ice edges and in summer (Arrigo et al., 1998). Even within regions dominated by a single taxon, however, both taxa are likely to co-exist (Smith and Asper, 2001).

Temporal and spatial gradients between *P. antarctica*- and diatom-dominated waters result from a combination of multiple physiochemical controls (Smith and Asper, 2001), including mixed-layer depths, micronutrients, and temperature distributions. For example, lower irradiance requirements of *P. antarctica* explain their dominance over diatoms in waters with deeper mixed layers (Kropuenske et al., 2009). Mixing of Circumpolar Deep Water with surface waters to produce Modified Circumpolar Deep Water (MCDW) has been hypothesized as a substantial source of iron to the assemblage, though a recent study has shown the Ross Sea iron budget dominated by benthic remineralization and sea ice input (D. McGillicuddy, pers. comm.). The timing and distribution of iron inputs may affect not only phytoplankton biomass, but also composition due to potentially distinct iron requirements of *P. antarctica* and diatoms. However, data on the relative requirements of each functional group are inconsistent (Alderkamp et al., 2012; Strzepek et al., 2012). Finally, higher temperatures have been correlated with higher diatom abundance, and lower temperatures with higher *P. antarctica* abundance (Liu and Smith, 2012), although it is not yet clear whether there is a causal mechanism behind this correlation.

Throughout the ocean, mesoscale processes on scales of 10–100 km and hours to days have first-order impacts on phytoplankton physiochemical controls, and are critical in determining growth patterns and distribution. For example, Friedrichs and Hofmann (2001) demonstrated how internal gravity waves, with periods of 6–8 days, can either stimulate growth or dilute chlorophyll concentrations in the euphotic zone by vertically advecting low-chlorophyll, iron-enriched water into the euphotic zone at rates greater than phytoplankton uptake. McGillicuddy et al. (2007) demonstrated that wind and eddy interactions could have varied effects on production at the mesoscale, with enhanced production associated with mode-water eddies and diminished production associated with cyclonic eddies. Indeed, the largest chlorophyll concentrations ever observed in the Sargasso Sea were associated with eddies (McGillicuddy et al., 2007). Finally Mahadevan et al. (2012) demonstrated that eddies generate mesoscale stratification in the North Atlantic to initiate the spring bloom prior to the effects of increased temperatures.

In the Ross Sea physical features such as tidal variations and wind-driven events have a substantial mesoscale impact on hydrodynamic variability. For example, diurnal tides produce continental shelf waves that, in turn, amplify shorter semidiurnal tides (Robertson, 2005). Variations in current velocity, salinity, and temperature have been attributed to this diurnal tidal forcing (Kohut et al., 2013). In addition, katabatic winds and synoptic forcing generate conditions favorable to atmospheric mesoscale cyclones over the Ross Sea (Heinemann and Klein, 2003). Episodic variations of wind speed and direction can lead to restratification as a result of Ekman advection across lateral density gradients (Long et al., 2012). Partly because of the difficulty obtaining high frequency observations within the Ross Sea, the effect of these physical processes on biological distributions is poorly known, but is likely to be significant. For example, the relief of irradiance limitation through stratification may be critically important to determining the timing and distribution of the seasonal phytoplankton bloom in the Ross Sea (Long et al., 2012).

Given the theoretical size of mesoscale features in the Ross Sea (10 km or less and on the order of days), such features cannot be well resolved by traditional oceanographic sampling from ships. However, autonomous underwater vehicles can successfully resolve this variability, as they have done in other regions of the Southern Ocean (e.g., Heywood et al., 2014). In the analysis presented here, an autonomous glider was deployed in the southern Ross Sea from December 2010 to January 2011 to characterize the biogeochemical mesoscale variability and highlight potential mechanisms contributing to this variability. We describe the glider deployment, sampling strategy, and ancillary data available for this analysis. The observed physical and biological distributions are presented along with significant correlations among these distributions; factors controlling these biological distributions are then discussed. Our results suggest a marked spatial, and presumably temporal, transition from a *P. antarctica*-dominated assemblage to one dominated by diatoms. Furthermore, frequent vertical penetrations of chlorophyll were observed, emphasizing the importance of mesoscale events to regional biogeochemistry.

2. Methods and data analysis

2.1. Glider platform

An iRobot Seaglider™ model 1KA (SN 502) completed two transects between 172.1°E and 179.9°W (~200 km) in the southern Ross Sea (Fig. 1) between December 19, 2010 and January 16, 2011. During this 28-day period, 370 dives were completed, 191 on the eastward section from December 19 through January 2, and 179 dives as the glider moved westward from January 2–16. The region surrounding the glider track was largely free of ice during both sections. Successive dives were separated by roughly 1 km, and extended to 600 m depth (except in shallower waters). The dives were divided into two portions, a down- and up-sampling phase, each of which were treated as separate "casts"; locations were computed for each cast as opposed to each dive. Because the glider obtains GPS positions only when at the surface, locations for down- and up-casts were interpolated to coordinates one-quarter and three-quarters, respectively, of the distance between the pre-dive and post-dive GPS-fixed locations. The glider's sensor suite provided measurements of conductivity and temperature (Seabird CTD), as well as fluorescence and optical backscatter (Wetlabs *Environmental Characterization Optics* Triplet Puck optical sensor

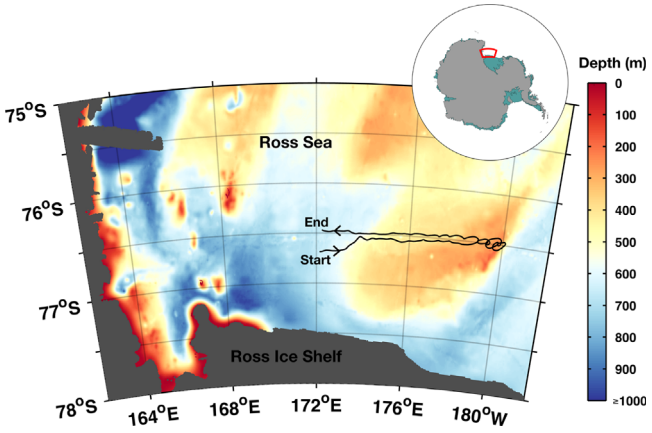

Fig. 1. Southwestern Ross Sea with glider track (black line). The glider's eastward (outbound) section began December 19, 2010, and the westward (return) section ended January 16, 2011. Gray areas represent topography above sea level or ice shelf. Bathymetric data obtained from the Bedmap2 dataset (Fretwell et al. 2013).

instrument). The Wetlabs optical sensor uses an LED excitation light source at 470 nm and detects fluoresced emissions at 695 nm, which is converted and output from the sensor in counts, ranging from 0 to 16,000. The optical sensor also measures backscatter within the same water volume at 470 nm and a centroid angle of 117°. Optical sampling frequency was once every 10 s in the upper 250 m, and switched off in deeper waters to conserve battery power. Temperature and salinity sampling frequency was once every 5 s in the upper 250 m and once every 10 s below 250 m. These data are available from the Biological and Chemical Oceanography Data Management Office (BCO-DMO) at http://www.bco-dmo.org/.

2.1.1. Physical data

A correction was applied to reduce hysteresis in the conductivity data at strong thermal gradients. When passing through a thermocline, thermal inertia in the conductivity cell of the sensor housing causes different response times for temperature and conductivity measurements (Lueck and Picklo, 1990). This effect is evident as slight salinity spikes of opposite signs on down- versus up-casts. The correction scheme devised by Morison et al. (1994) and refined by Garau et al. (2011) was used to reduce hysteresis. To lessen the spikes further, an 8 m running median was applied and salinities were binned every 1 dbar.

Mixed layer depth (MLD) was determined for each cast by a potential density threshold using three different methods. The first two methods utilized simple potential density threshold criteria; specifically, MLD was defined as the shallowest depth at which σ_θ differed from the value at 10 m by 0.01 kg m^{-3} in the first method and by 0.03 kg m^{-3} in the second method. This type of methodology is consistent with other Ross Sea studies, which have used density thresholds ranging from 0.01–0.1 kg m^{-3} (Smith and Gordon, 1997; Sedwick et al., 2011; Smith et al., 2011a). The MLD was also computed using the maximum angle method, which was applied by Chu and Fan (2011) to glider data from the Florida coast and found to be more objective than threshold or gradient methods and less confounded by noisy data than curvature methods. The maximum angle method involves pairs of vectors being fit, by linear regression, head-to-end along consecutive sections of an entire depth–density profile. The tangent of the angle between each pair of vertically adjacent vectors is calculated. The MLD is then determined to be the depth that lies between the vector pair with the maximum angle. Differences between the three aforementioned methodologies for computing MLD were found not to substantially affect interpretation of MLD results; therefore, only the calculation via the 0.01 kg m^{-3} difference σ_θ threshold was used in the statistical analyses.

MCDW was determined to be present if neutral density (Jackett and McDougall, 1997) was between 28.00 and 28.27 kg m^{-3} (Orsi and Wiederwohl, 2009). This neutral density criterion was supplemented by an additional criterion of low dissolved oxygen (Budillon et al., 2003; Fragoso and Smith, 2012; Kohut et al., 2013). Specifically, MCDW was positively identified at a given location if the above limits on neutral density were satisfied and the water was determined to be at less than 80% of oxygen saturation. [Contemporaneous dissolved oxygen data were available from the glider and are presented and analyzed in Queste (2014)]. Ranges of depths where water met these two MCDW criteria were identified for each cast, and vertical surface areas were computed for each section by horizontally integrating the depth ranges of MCDW across cast longitudes.

2.1.2. Biological data

Glider fluorescence counts obtained from the Wetlabs sensor were converted to chlorophyll via calibration with ship data collected during glider recovery. Specifically, the fluorescence profile from the last glider up-cast was regressed with shipboard bottle chlorophyll measurements from the recovery station (76.4°S, 173.2°W). The regression was computed to be: CHL = (Fluorescence − 141)*0.00225 ($n=12$, $R^2=0.94$, $p<0.01$).

A similar ship-based calibration process was used to convert optical backscatter values obtained from the Wetlabs optical sensor to POC concentrations. Raw scattering counts minus dark counts were converted to total volume scattering, β (117°,470 nm) using a factory-calibrated scale factor. Total volume scattering was converted to particulate volume scattering coefficients, β_p, by subtracting the volume scattering of seawater, β_w (Morel, 1974), and then converted to particulate backscattering b_{bp} (470 nm), by a factor of $2\pi\chi$, where χ is 1.1 (Boss and Pegau, 2001). The resulting particulate backscattering (b_{bp}) profile from the last glider up-cast was regressed with shipboard POC measurements of water samples. The resulting POC regression relationship (POC = 19,607*b_{bp} + 17.621; $n=11$, $R^2=0.85$, $p<0.01$) was used to determine concentrations for all glider casts.

2.2. Ancillary data

Chlorophyll and POC concentrations for use in the regression analyses described above were determined from water samples collected from the *RVIB Nathaniel B. Palmer* (NBP11-01) using a SeaBird CTD/rosette system. Samples from known depths were placed in opaque bottles and filtered under low pressure (~1/3 atm) through Whatman GFF filters (POC filters were precombusted at 450 °C for 2 h). Chlorophyll samples were placed in cuvettes with 7 mL 90% acetone, extracted in the cold (−20 °C) and dark for 24 h, and then quantified by fluorescence on a Turner Designs Model 10 AU fluorometer that had been calibrated with commercially prepared chlorophyll *a* (Sigma). The POC samples were dried at 60 °C in combusted glass vials, returned to the laboratory and analyzed via pyrolysis on a Costech ECS 4010 elemental analyzer. Blanks were filters through which filtered seawater had been run (ca. 5 mL) and treated in the same manner (Gardner et al., 2000).

Wind speeds at 10 m height were retrieved every six hours from European Centre for Medium-Range Weather Forecasts (ECMWF) ERA-Interim reanalysis data gridded by 0.75 × 0.75° over the locations and times of each glider cast (http://apps.ecmwf.int/datasets/data/interim_full_daily/; Dee et al., 2011). The ocean color and sea surface temperature data projected on a 9 km spatial grid for December 2010 and January 2011 were retrieved as Level 3 Standard Mapped Image monthly composites of Aqua Moderate Resolution Imaging Spectroradiometer (MODIS) from the OceanColor Web (http://oceancolor.gsfc.nasa.gov/), distributed by the NASA Ocean Biology Processing Group. Due to extensive cloud cover throughout the study period, only two days during the study period provided usable ocean color data for more than half of the southwestern Ross Sea; hence, a comparison of glider observations and satellite-derived data on higher resolution temporal scales was not feasible. Uncertainties in satellite derived chlorophyll concentrations in the Ross Sea are estimated to be ~65% (Saba et al., 2011).

2.3. Statistical analyses

Mean section values were calculated from longitudinally binned (0.25°) glider observations (Table 1). Pearson linear correlation coefficients (Sokal and Rohlf, 1969) were computed using raw data for each variable pair across the eastward and westward sections as well as the entire glider track (Table 2). Correlation coefficients were also calculated for variable pairs after subsampling the data at resolutions similar to that of traditional cruise

Table 1
Mean and integrated values computed using 0.25 km binned data from the eastward and westward glider sections. Standard deviations are presented in parentheses for mean values. All eastward and westward section means were found to be significantly different ($p < 0.05$). Integrated MCDW areas were not tested for significance.

Variable	Eastward section	Westward section
Mean SST (°C)	−0.62 (0.19)	−0.22 (0.41)
Mean MLD (m)	19 (4)	26 (7)
Integrated MCDW area (km^2)	11	13
Mean wind speed ($m\ s^{-1}$)	3.2 (1.2)	6.1 (3.2)
Mean chlorophyll in mixed layer ($mgChl\ m^{-3}$)	2.3 (0.6)	1.3 (0.7)
Depth-integrated (0–150 m) Chl ($gChl\ m^{-2}$)	0.40 (0.051)	0.27 (0.075)
Mean POC in mixed layer ($mgC\ m^{-3}$)	76 (7.9)	101 (46)
Depth-Integrated (0–150 m) POC ($gC\ m^{-2}$)	10 (0.66)	11 (1.4)
Mean POC:Chl ratio in mixed layer ($mgC\ (mgChl^{-1})$)	47 (13)	105 (41)

Table 2
Pearson linear correlation coefficients for pairs of variables. Dashed lines represent insignificant correlations. Bold numbers highlight correlations greater than 0.5.

	Mean Chl in mixed layer	Mean POC in mixed layer	Mean POC:Chl in mixed layer
Whole track			
SST	**−0.73**	0.35	**0.83**
MLD	0.16	0.38	0.11
MCDW thickness	**−0.53**	−0.20	0.32
Wind speed	−0.42	**0.61**	**0.69**
Eastward/outbound section			
SST	−0.43	---	0.49
MLD	0.35	---	−0.39
MCDW Thickness	−0.34	---	0.29
Wind Speed	---	0.15	0.11
Westward/return section			
SST	**−0.78**	0.33	**0.86**
MLD	0.38	0.46	---
MCDW thickness	**−0.71**	−0.33	0.37
Wind speed	−0.37	**0.63**	**0.68**

Table 3
Pearson linear correlation coefficients for pairs of variables from subsampled (~50 km) data. The two numbers in each cell represent correlations from subsampled station sets offset by 9 km. Dashed lines represent insignificant correlations. Bold numbers highlight correlations greater than 0.5.

	Mean Chl in mixed layer	Mean POC in mixed layer	Mean POC:Chl in mixed layer
Whole track			
SST	---,---	---,---	---,**0.84**
MLD	---,---	---,---	---,---
MCDW thickness	---,**−0.73**	**---,---**	---,**−0.74**
Wind speed	---,**−0.73**	---,---	**0.69**,**0.96**
Eastward/outbound section			
SST	---,---	---,---	---,---
MLD	---,---	---,---	---,---
MCDW thickness	---,---	---,---	---,---
Wind speed	---,---	---,---	---,---
Westward/return section			
SST	---,---	---,---	---,---
MLD	---,---	---,---	---,---
MCDW thickness	---,---	**---**,**0.83**	---,**0.95**
Wind speed	---,---	---,---	---,**0.95**

stations (Table 3; see Section 4.2). A priori correlations with p values ≤ 0.05 were considered statistically significant.

3. Results

3.1. Physical properties

Significant differences were found between the temperature and MLD data from the eastward/outbound track (December 19–January 2) and the westward/return track (January 2–16). For example, sea surface temperature (SST; the average temperature of the upper 5 m) was 0.4 °C cooler along the eastward/outbound section than along the westward/return section (Table 1). Although a general warming trend would be expected during summer, there was a particularly strong increase in SST between January 3–7 (Fig. 2a). Monthly satellite composites from December 2010 and January 2011 set these glider SST data in a broader spatial context (Fig. 3). The December 2010 image shows almost no spatial temperature gradient along the glider track, whereas the January 2011 image indicates significantly cooler surface temperatures in the eastern half of the glider track compared with the western half. The January image (Fig. 3b) also corroborates the surface glider data (Fig. 2a), showing slightly warmer temperatures on the return (northern) track compared with the outbound (southern) track. The glider profile data (Fig. 4) provide a view of the deep temperature structure beneath these surface waters, and illustrate the significant mesoscale variability within the temperature field. Surface temperatures routinely change by more than 0.5 °C on very short time (O(1 h)) and space (O(1 km)) scales, and pulses of warm surface water periodically penetrate below 50 m for brief (O(1 h)) intervals.

Despite the consistently cold temperatures (< -1.5 °C) in deep waters, warmer surface temperatures on the return track were associated with deeper MLDs: on average MLDs were ~7 m deeper on the warmer, westward/return section (Table 1; Fig., 2b). However, there was a general shoaling of the MLD concurrent with the January 3–7 warming event (Fig. 2a,b). MLD deepened again during January 10–13, a period with stronger wind forcing (Fig. 2b, d). In general, defining MLD using the $\sigma_\theta = 0.01\ kg\ m^{-3}$ difference threshold produced MLDs that were consistent with the depth of the thermocline (Fig. 4). The exception occurred on January 8–9, during which time the isothermal layer depth was consistently deeper than MLD estimated by the σ_θ criterion, suggesting that changes in salinity were affecting MLD during this period.

Although SST and MLD were significantly different between the eastward/outbound section and the westward/return transect, the

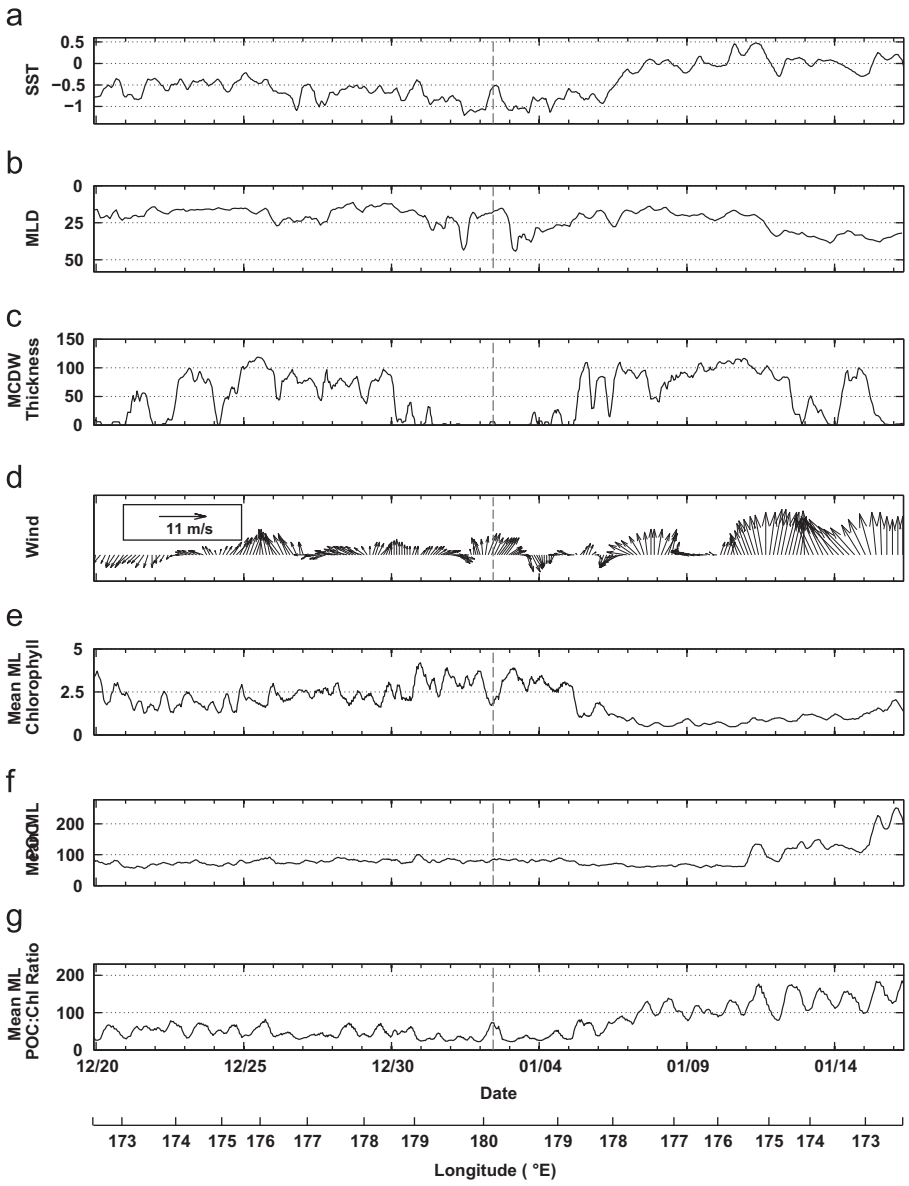

Fig. 2. Temporal and spatial distribution of (a) sea surface temperature (°C), (b) mixed layer depth (m), (c) depth thickness of MCDW (m), (d) 10 m wind speed (m s^{-1}) and direction, (e) mean mixed layer chlorophyll concentration (mgChl m^{-3}), (f) mean mixed layer POC concentration (mgC m^{-3}), and (g) mean mixed layer POC:Chl ratio (mgC ($mgChl^{-1}$)). Vectors directed to the top of the page in (d) represent southerly winds. All time-series lines are 5-point moving averages. The vertical dashed line located between January 2 and January 3 demarcates the eastward section (to the left of the line) from the westward section (to the right of the line).

distribution of MCDW identified by the glider was similar within both transects (Table 1). For example, in both sections (Figs. 2c, 4) MCDW was most prominent in the central portion of each section (~173–179°E). The vertical surface area (see Section 2.1.1) in which MCDW occurred increased from the eastward to the westward section: 11 km^2 to 13 km^2 (Table 1). (For comparison, each section, with a horizontal distance of 203 km and average depth of 363 m, had a total vertical surface area of ~74 km^2.) Within both sections the deepest MCDW was located between 175 and 176°E at the western edge of Ross bank (Figs. 1 and 4). MCDW then became progressively shallower over the bank, following the bathymetric gradient, with the shallowest occurrences of MCDW in both sections located near the shallowest portions of the bank, on its eastern edge between 178 and 179°E. Significant mesoscale variability is also apparent. For example, a mixing event that occurred on January 6 not only resulted in warmer waters below 100 m, but also simultaneously eliminated all evidence of MCDW at this depth (Fig. 4b).

Significant mesoscale variability in this region is associated with the wind field. Wind speeds at the specific location of the glider were approximately 3 m s^{-1} lower when the glider was traversing the eastward/outbound section compared with the wind speeds when the glider was returning on the westward section (Table 1). Throughout much of the glider track wind speeds remained less than or equal to ~5 m s^{-1}; however, they nearly doubled around January 10 (Fig. 2d), whereupon the winds became consistently strong for the remainder of the section. Winds were predominantly southerly for both sections, with the exception of the first few days (December 19–22) and brief intervals on January 4 and 6, which were characterized by winds from the north.

3.2. Biological distributions

Substantial changes in chlorophyll distributions were observed along the glider track. Overall, mean chlorophyll concentrations in

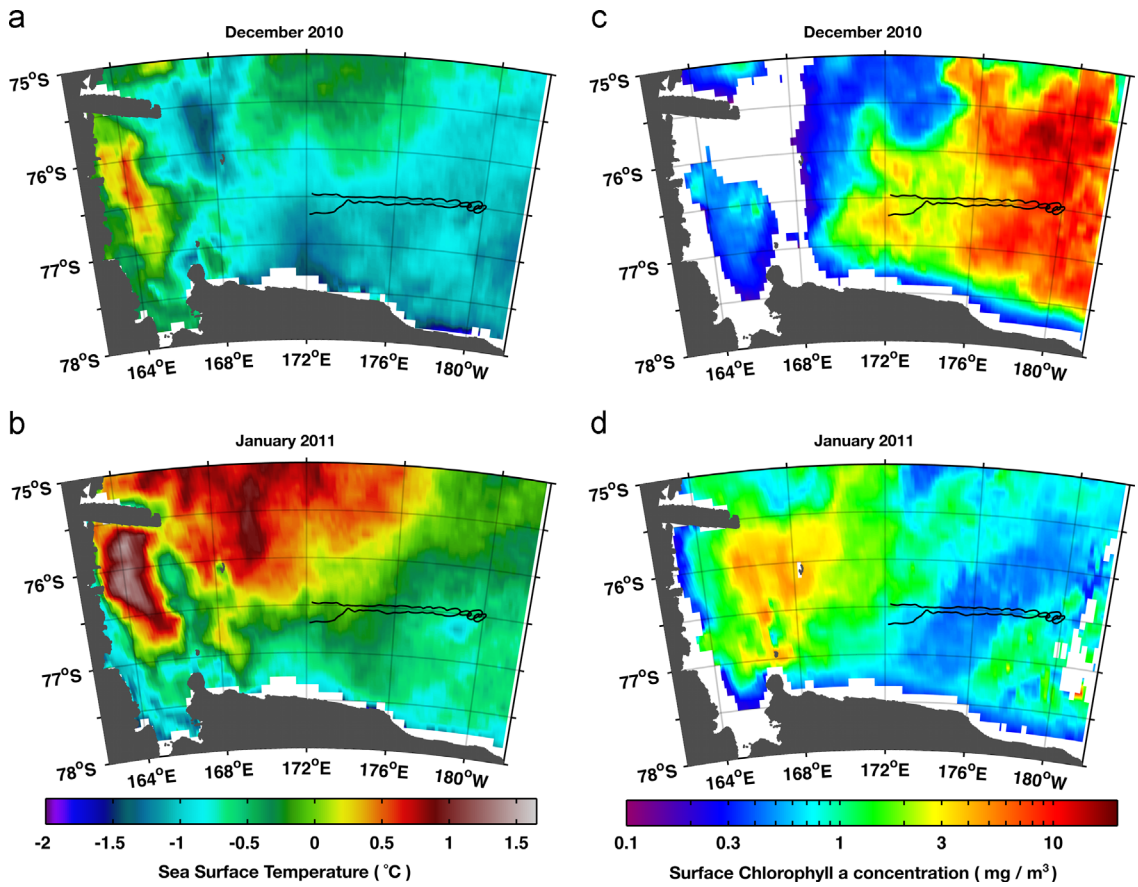

Fig. 3. MODIS images of the southwestern Ross Sea of monthly composites of SST for (a) December 2010 and (b) January 2011 and chlorophyll concentrations for (c) December 2010 and (d) January 2011. The thin black lines illustrate the location of the glider track. The white areas in (c) and (d) roughly represent locations where mean monthly ice cover exceeded 50%. Gray areas represent topography above sea level or ice shelf.

the mixed layer were 1 mg Chl m^{-3} higher on average during the outbound section than during the return section, and depth-integrated (0–150 m) chlorophyll concentrations showed a similar trend (Table 1). Mean chlorophyll concentrations in the mixed layer were relatively constant during the outbound track in December, but changed significantly in January. First there was a marked decrease in mixed layer chlorophyll during January 3–7 (Fig. 2e), concurrent with the SST increase previously described. Mixed layer chlorophyll then remained low until the end of the westward occupation (January 13–16), whereupon a modest increase in mixed layer chlorophyll was observed (Figs. 2e and 6b). Satellite-derived chlorophyll concentrations show the opposite trend. A significant longitudinal chlorophyll gradient existed in December, with higher chlorophyll in the eastern half of the glider track and lower values in the western half (Fig. 3c). By January, however, this spatial gradient in surface chlorophyll had disappeared, and the satellite-derived data show low surface concentrations and minimal spatial variation along the glider track (Fig. 3d). This inconsistency in chlorophyll variability as observed by the glider versus the satellite likely results from the fact that chlorophyll evolves on time scales less than the ~2 weeks between repeated observations of the glider sections. The satellite data also do not represent monthly averages, but instead represent the average of a few cloud-free days in December and January. Furthermore, surface fluorescence-derived chlorophyll values from the glider are not directly comparable to satellite estimates because much of the surface variability reflects diel quenching rather than in situ concentration changes (see Section 4.1.1).

Concentrations of POC were similar between the two sections except for an abrupt change near the end of the westward/return track. This change caused mean mixed layer POC in the outbound track to be 25 mg m^{-3} lower on average than during the return track (Table 1). Integrated POC concentrations were remarkably consistent throughout both the eastward and westward sections (Table 1), and it was only after January 10 (and west of 176°E) that mixed layer concentrations increased abruptly, reaching maximum values on January 15 (Figs. 2f, 6). This increase in POC concentrations occurred ~3–7 days after the decrease in mixed layer chlorophyll, but at approximately the same time as the decrease in the deep chlorophyll signal and the increase in southerly winds (Figs. 2d–f, 5, and 6).

Mesoscale variability of both chlorophyll and POC concentrations was also evident below the mixed layer throughout both sections (Figs. 5, 6). Chlorophyll and POC both episodically penetrated to depths of ~100–200 m on short (O(1 h)) time scales. A close examination of Figs. 5 and 6 reveal that these events co-occurred (i.e., both POC and chlorophyll were elevated at depth simultaneously). The deep chlorophyll and POC signal (below 75 m) decreased on January 10, at the same time as the surface POC concentration increased. Deep chlorophyll and POC concentrations then remained low until the end of the glider track (Figs. 5b, 6b). In general, deep chlorophyll and POC concentrations varied in phase, whereas mixed-layer concentrations were largely out of phase, with the highest POC concentrations occurring at times of lowest chlorophyll concentrations.

The ratio of POC to chlorophyll in the mixed layer remained fairly constant during the eastward/outward track, but changed greatly during the westward/return track. On average, POC:Chl during the westward track was approximately double that of the eastward track (Table 1). The POC:Chl began increasing as mixed layer chlorophyll decreased (January 3–7) and continued

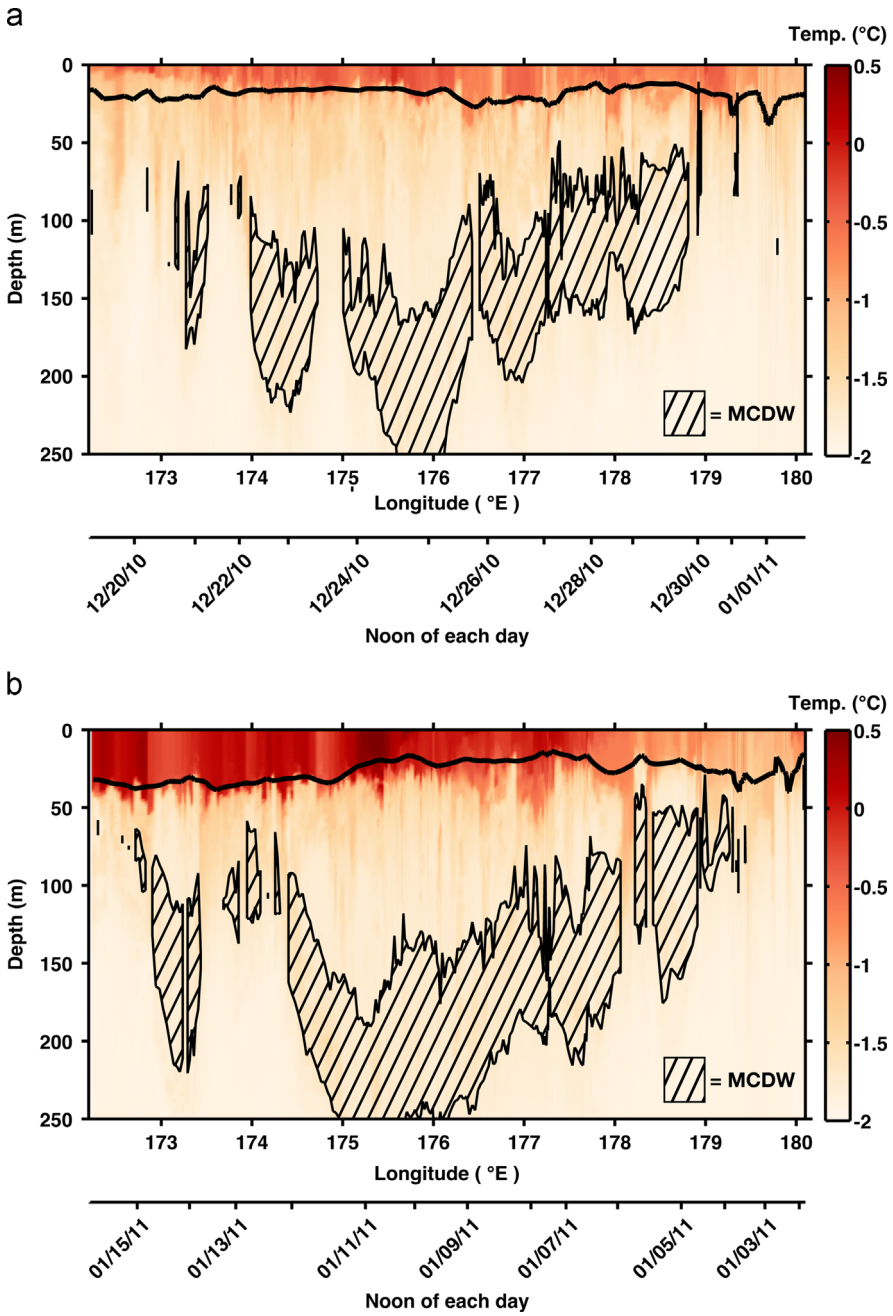

Fig. 4. Temperatures during the (a) eastward/outbound and (b) westward/return glider sections. The thick black line represents a 5-point moving average of mixed layer depth and hatched areas represent MCDW.

increasing through the later period of increasing POC (January 10–15); over this almost two week period, POC:Chl increased approximately two-fold (Fig. 2g) at a rate of ~15 mgC $mgChl^{-1}$ per day. By the end of the westward track, the POC:Chl ratio had reached a maximum value of approximately 230 mgC $mgChl^{-1}$, increasing from an average value of 47 mgC $mgChl^{-1}$ during the eastward section.

3.3. Correlations

Correlation coefficients were calculated between physical variables (SST, MLD, MCDW thickness and wind speed) and biological variables (mixed layer chlorophyll, POC and POC:Chl ratio) across the whole glider track (Table 2). Mixed layer depth was not highly correlated (correlations < 0.4) to chlorophyll or POC. In contrast, average mixed layer chlorophyll was most strongly correlated (−0.73) with SST: higher chlorophyll concentrations were associated with colder temperatures. To a lesser degree, chlorophyll was also inversely correlated with MCDW thickness (−0.53) and wind speed (−0.42), such that higher chlorophyll concentrations were associated with low winds and occurred where MCDW influence was low. In contrast to chlorophyll, which was relatively highly correlated to multiple physical variables (SST, MCDW and wind), POC concentrations were only highly correlated (0.61) with winds over the whole track: significantly higher POC concentrations occurred when wind speeds were high (Fig. 2). The ratio of POC:Chl in the mixed layer was strongly positively correlated with both SST (due to chlorophyll) and wind speed (due to the POC contribution.)

Correlation coefficients were also calculated separately for data within each section (Table 2). The westward/return section correlations exhibited similar correlations as were found for the entire track, with strong inverse correlations of chlorophyll and SST and

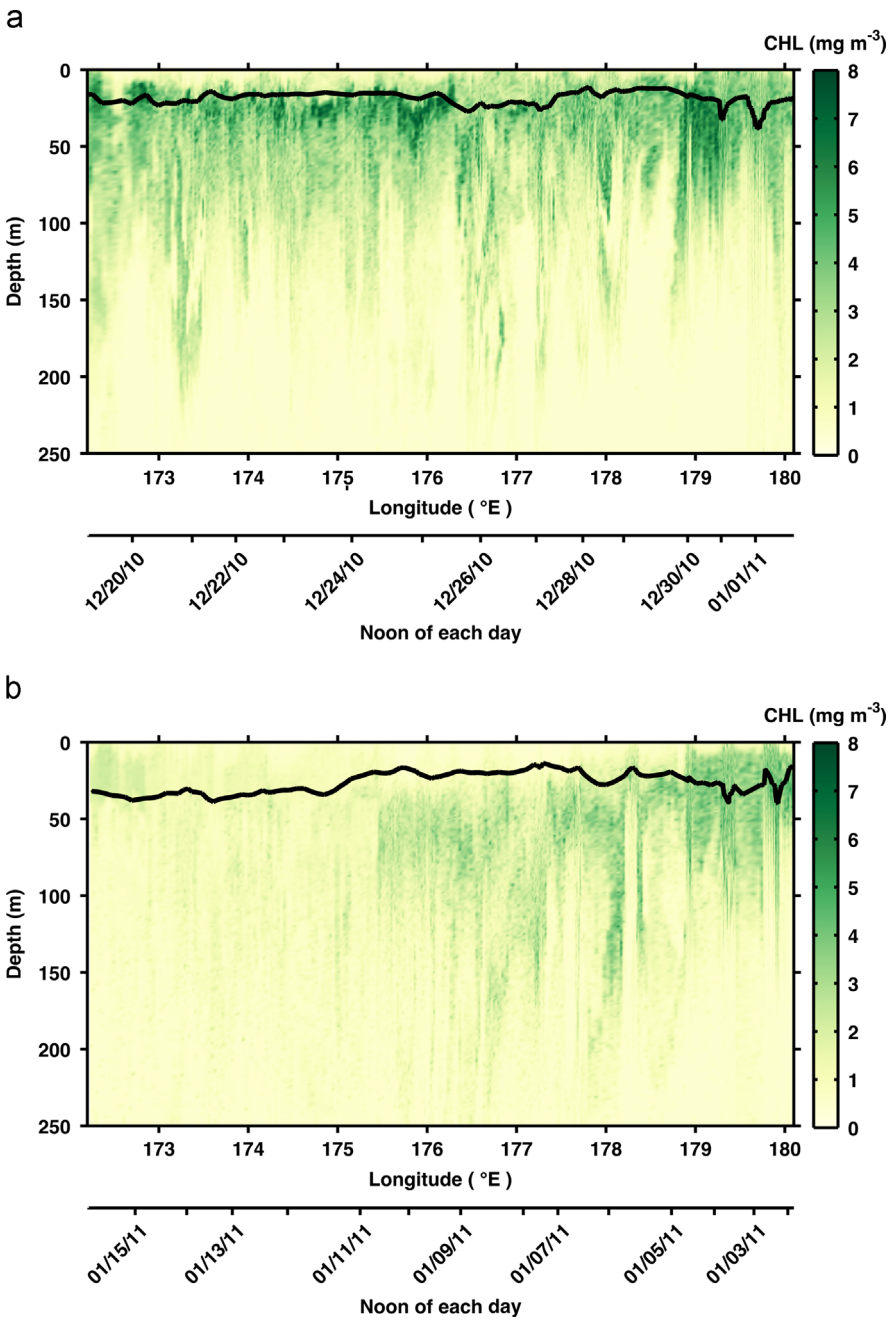

Fig. 5. Fluorescence-derived chlorophyll concentrations during the (a) eastward/outbound and (b) westward/return glider sections. The thick black line represents a 5-point moving average of mixed layer depth.

strong positive correlations between POC and wind speed. In addition, on this westward section POC was strongly positively correlated with MLD, such that high POC concentrations were associated with deep mixed layers. Although the strong inverse correlation between chlorophyll and SST was also apparent on the eastward track, POC was not highly correlated to any physical variables on the eastward track.

4. Discussion

4.1. Factors controlling observed chlorophyll and POC distributions

Multiple physical and biological processes are known to play a role in the variability of the original fluorescence and backscatter data of the glider, and may explain some of the variability in the derived concentrations of chlorophyll and POC, respectively. For example, diel variations in near-surface fluorescence may be related to diurnal shifts from photochemical quenching to non-photochemical quenching. Moreover, variations in deep chlorophyll may represent sinking and export of *P. antarctica*. Abrupt changes in the ratio of POC to chlorophyll potentially suggest a shift in phytoplankton composition. Although MCDW and MLD were expected to play major roles in controlling biological distributions in the Southern Ross Sea, neither played as significant a role as that of wind and SST on the time/space scales measured by the glider. The influence of these multiple factors on fluorescence and backscatter, hence on the derived chlorophyll and POC and their variability, is described below.

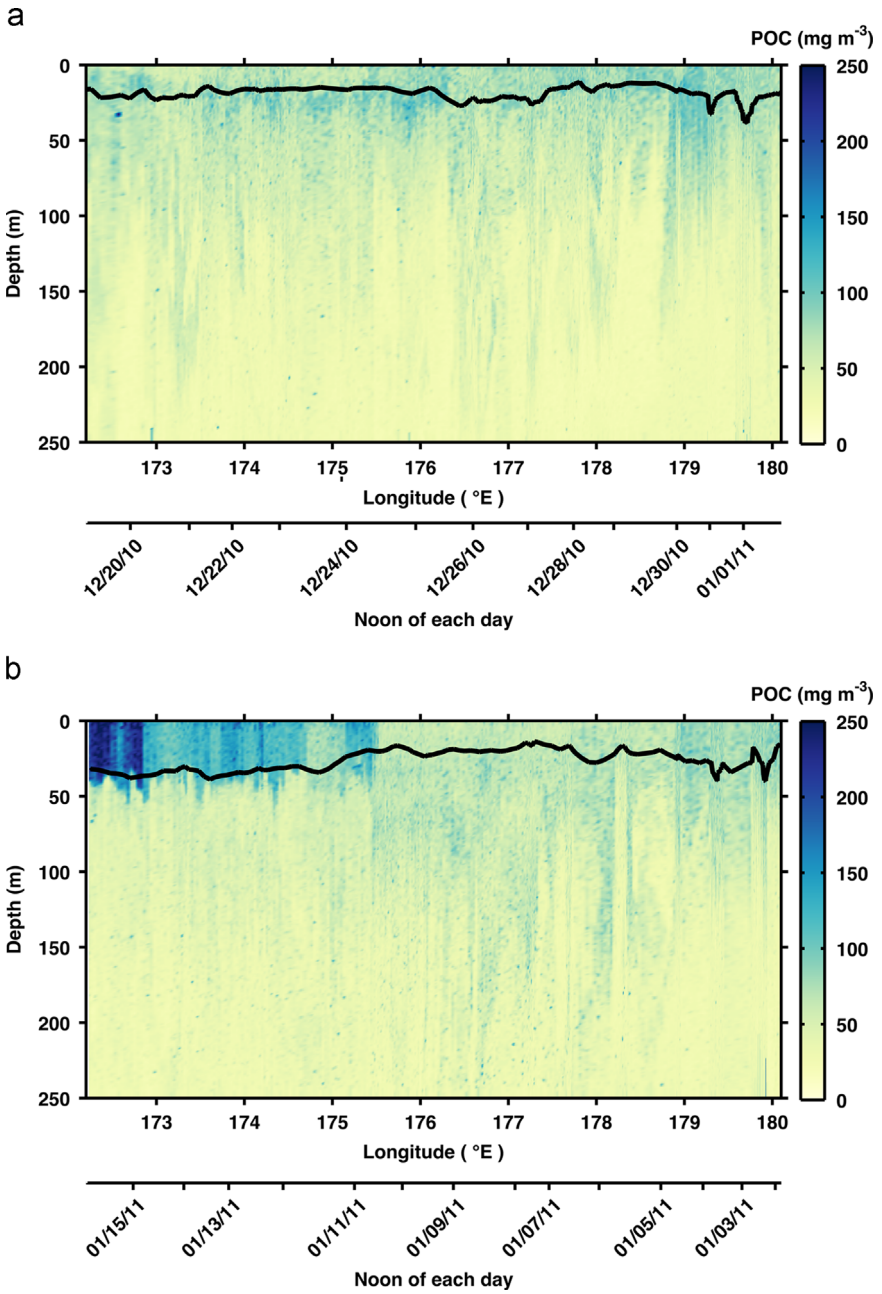

Fig. 6. Optical backscatter-derived particulate organic carbon concentrations during the (a) eastward/outbound and (b) westward/return glider sections. The thick black line represents a 5-point moving average of mixed layer depth.

4.1.1. Diel fluorescence cycles

The high-resolution measurements obtained by the glider revealed diel cycles of fluorescence, with minima occurring around noon and maxima near midnight (Fig. 7). Previous studies have shown that maximum fluorescence yield of phytoplankton cells can be decreased, or quenched, by release of energy as heat, and this process is termed non-photochemical quenching (NPQ; Buschmann, 1999). Photoinhibition and photoprotective NPQ can occur when cells are subject to high mid-day irradiance (Van de Poll et al., 2011), and the diel pattern of fluorescence observed by the glider likely results from such quenching. A similar pattern has been observed in moored fluorometry data from the same region, and is evident even during 24-h photoperiods (Smith et al., 2011a). Fluorescence also decreased slightly near midnight during numerous periods, a pattern similar to nocturnal depressions previously hypothesized (Behrenfeld et al., 2006). Behrenfeld et al. (2006) suggested that nocturnal depressions are unlikely to occur in polar regions, but the occasional occurrence of this pattern in these data suggests that summer mid-night depressions may also be possible in polar systems and may reflect a reduction in the plastoquinone pool at night.

4.1.2. Modified Circumpolar Deep Water

It has been hypothesized that the presence of MCDW in subsurface layers of the Ross Sea stimulates surface productivity by providing iron that relieves micronutrient limitation (Hiscock, 2004; Peloquin and Smith, 2007). Hiscock (2004) found a strong spatial correlation with his delineation of MCDW based solely on neutral density and pigment concentrations derived from coarse-resolution (~50 km station spacing) shipboard data. In contrast, the results obtained here, which are generally consistent with results obtained using other platforms during the 2010–2011 season (Smith et al., 2014), do not indicate

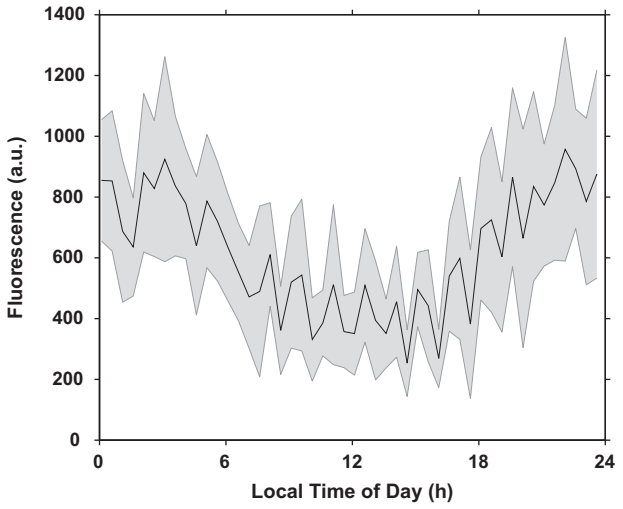

Fig. 7. The average diel cycle of fluorescence; data are binned every half-hour. The black line shows mean fluorescence (in arbitrary units of output counts) at 5 m depth, and the shaded region indicates the ±95% confidence interval.

any such positive correlation between mixed layer chlorophyll or POC concentration and the appearance of MCDW, its depth, or the portion of the water column that it occupies. The absence of a positive correlation suggests that MCDW is not stimulating phytoplankton growth during summer; however, it is not clear whether this is due to an insufficient supply of iron associated with the MCDW or whether iron is simply not limiting phytoplankton growth at this particular time and place.

4.1.3. Mixed layer depth

Estimates of MLD vary according to method used for calculation and are affected by several distinct processes. Numerous procedures exist for identifying MLD, including thermal difference and gradient, shape of the density profile, and dissolved O_2 criteria (Chu and Fan, 2011; Holte and Talley, 2009; de Boyer Montégut et al., 2007). Algorithms that rely on temperature alone or potential density reveal mixing effects of dissimilar water column processes (de Boyer Montégut et al., 2004), with dissolved O_2 being additionally affected by air-sea gas exchange and biological processes (Castro-Morales and Kaiser, 2012). In this study, using different potential density thresholds did not substantially affect the results. In addition, the computed MLDs are not significantly correlated to the glider SSTs, so that the expected pattern of higher SST linked with shallower MLD is not apparent. Factors that affect MLD, such as wind, buoyancy, ice melt, and waves (Belcher et al., 2012), may be responsible for the lack of correlation with SST in these data.

In the open waters of the central Ross Sea, mixed layer depths are generally relatively deep and phytoplankton assemblages are primarily dominated by *P. antarctica*, which typically exhibit relatively low POC:Chl ratios (DiTullio and Smith, 1996); in contrast, diatoms, which exhibit relatively high POC:Chl ratios, dominate in shallower mixed layer regions characteristic of ice edges (Arrigo et al., 1999; Smith et al., 2010). On the time and space scales observed by the glider during 2010–11, a contrasting pattern emerged: the glider data revealed higher POC:Chl ratios during relatively deep (30–50 m) mixed layer conditions. By means of a pigment analysis, Fragoso and Smith (2012) found a similarly contrasting pattern. They found diatoms dominating the assemblage when deep mixed layers were present in late summer, and suggested that the MLD–composition relationship was temporally and/or spatially variable. Together, these studies seem to indicate that although diatoms tend to be present in locations that are generally characterized by relatively shallow mixed layer depths, the temporal variability of these concentrations at a given location is such that higher diatom concentrations are sometimes associated with deeper mixed layer depths. However, the mechanisms generating these observed diatom distribution patterns require further study.

4.1.4. SST and wind

Although biological distributions (chlorophyll, POC) were not highly correlated to MLD or the presence of MCDW, these biotic distributions were highly correlated with SST and wind speed. Specifically, cold temperatures were associated with high chlorophyll concentrations and high winds were associated with high POC concentrations (Table 2). The association between SST and chlorophyll appears linked to the seasonally increasing temperatures and waning phytoplankton bloom; seasonally increasing SSTs are evident in both the glider SST observations (Figs. 2a and 4) and satellite SST composites (Fig. 3a,b). This description is consistent with Liu and Smith's (2012) analysis of four years of cruise data, which exhibited a strong, inverse association between *P. antarctica* and temperature and more minor contributions to biological variance from water column stratification.

In addition to the background seasonal warming, substantial mesoscale variability caused temperature gradients on shorter time and space scales as well. For example, the abruptly warming surface temperatures observed between January 3 and 7 are associated with abruptly decreasing chlorophyll concentrations during this same period. Although it is not possible to ascertain the cause of the temperature increase, it is likely associated with a series of consecutive sunny days. Net solar radiation reanalysis fluxes provided by the National Center for Environmental Prediction (http://www.esrl.noaa.gov/psd/data/gridded/data.ncep.reanalysis.html; Kalnay et al., 1996) at 178°E indicate that the only period of five consecutive days with net shortwave radiation fluxes $>300\ W\ m^{-2}$ at this location occurred during the time period of January 3–6. In contrast, the preceding time period (December 23–31) averaged $\sim 230\ W\ m^{-2}$. Such an increase in solar radiation would be expected to decrease fluorescence through acclimation to high irradiance conditions characteristic of highly stratified conditions, whereas the concentration of chlorophyll may not necessarily be affected, although the degree of this effect would depend upon phytoplankton composition (Kropuenske et al., 2009). Such a decrease in fluorescence-derived chlorophyll was observed in January 2011 as the glider moved into waters with a deeper overall water column, and these same waters were characterized by relatively low surface chlorophyll concentrations as measured by satellite (Fig. 3c,d).

Concentrations of POC observed by the glider were nearly constant between the time of the deployment until January 11. At this time, a substantial increase in POC occurred contemporaneously with a doubling of wind speed, which was then followed by a discernable deepening of the mixed layer. The significant correlation between wind speed and POC suggests a vertical mixing effect, perhaps through changes in irradiance availability and/or nutrient redistribution. Frequent mesoscale mixing events in the Ross Sea have previously been associated with substantial biological variability, and may transform the assemblage by altering the irradiance environment (Smith et al., 2011a). Although the higher POC concentrations could also be explained by the horizontal advection of POC-rich water into this region, this would require an explanation for increased POC in neighboring waters.

4.1.5. Phytoplankton composition

It is possible that the observed chlorophyll decrease (January 3–7) and POC increase (after January 10) could represent a change

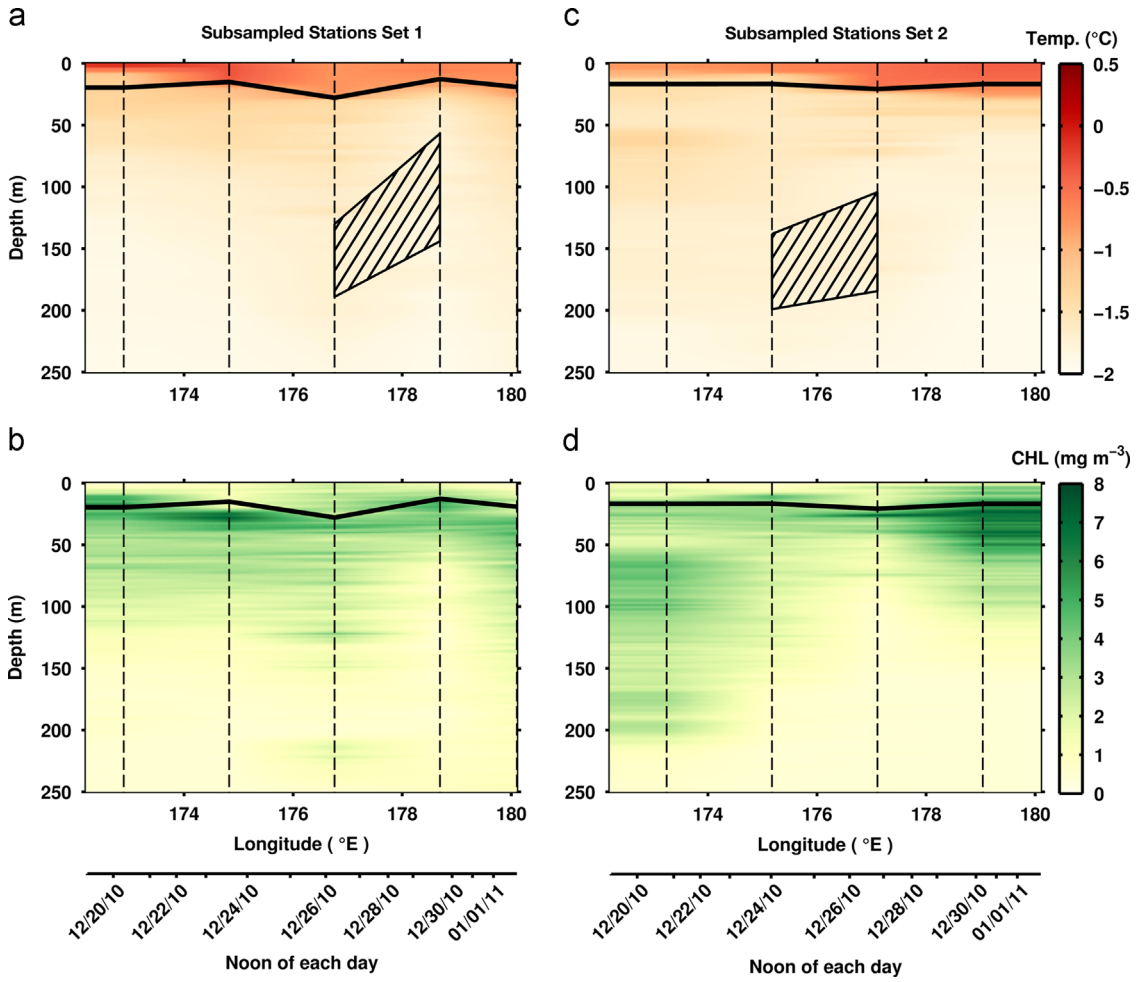

Fig. 8. Eastward glider sections sub-sampled at reduced horizontal resolution (~50 km station spacing) for temperature (a, c) and fluorescence-derived chlorophyll (b, d). Two different subsampled station sets are used (a,b vs. c,d, offset by 9 km, as illustrated by dashed lines) to calculate mixed layer depths (thick black lines) and MCDW (hatched areas), and the specific locations of the selected stations strongly affect the contoured chlorophyll distributions.

in the contributions of solitary versus colonial cells of *P. antarctica*. Since colonies partition substantial amounts of carbon to mucus (Mathot et al., 2000), a transition from solitary to colonial cells might be expected to result in an increase in POC:Chl ratio. However, the fraction of *P. antarctica* that is composed of mucilaginous colonies is generally highest in December (Smith et al., 2000), and decreases as the colonies sink and solitary flagellated cells are released (Mathot et al., 2000). Furthermore, the number of solitary cells remains relatively low during summer, likely as a result of microheterotroph grazing (Smith et al., 2003). If the glider data were capturing such a shift from colony-dominated to solitary-cell dominated *P. antarctica* at one depth, a decrease in the POC:Chl would be expected, opposite to what is observed. Thus, it is unlikely that the changes in bio-optical data reflect a change in the relative contributions of solitary cells of *P. antarctica*. Although higher POC:Chl ratios could also be explained by an increase in detrital matter, detrital carbon amounts are considered to be low in the Ross Sea during this time of the year (Mathot et al., 2000), and thus this is also not a likely explanation for the observed decrease in chlorophyll and increase in POC. Finally, as grazing is generally understood to have limited effect on phytoplankton assemblages in the Southern Ross Sea (Caron et al., 2000; Dennett et al., 2001; Tagliabue and Arrigo, 2003), herbivory is unlikely to be responsible for the observed variability.

Another potential explanation for the observed changes in the POC:Chl ratio is that iron limitation became more severe, as iron inputs are largely restricted in summer in the Ross Sea (Sedwick et al., 2011), and the phytoplankton responded by altering intracellular ratios. Nutrient limitation often impacts chlorophyll synthesis before growth and overall biomass, and the increased ratios observed by DiTullio and Smith (1996) are consistent with iron limitation. Furthermore, increased POC:Chl ratios observed in mesocosms of *P. antarctica* in the Ross Sea were observed after nutrient depletion (Smith et al., 1998), which is again consistent with the hypothesis of a physiological acclimation to nutrient limitation.

Finally, another potential explanation for the observed decrease in chlorophyll and subsequent increase in POC is that the glider was witnessing a transition from *P. antarctica* to diatoms. Although gliders do not provide accessory pigment information or samples for microscopic species identification, the results presented here suggest that compositional changes in the biota likely played a role in the observed variations in optical data. For example, the observed changes in POC and chlorophyll concentrations are characteristic of a shift in phytoplankton assemblage, as low POC, high chlorophyll waters throughout the eastward section gave way to higher POC and low chlorophyll waters during the westward section. Such differences between low and high POC:Chl ratios have been observed previously in the Ross Sea (DiTullio and Smith, 1996) and were found to be distinguishing features of *P. antarctica*-dominated and diatom-dominated assemblages, respectively. Both spatial and temporal gradients may have played

a role in the observed variability. It is possible that there were two spatially separated blooms, as evident in MODIS satellite imagery (Fig. 3c,d), and the movement of the glider through this spatial arrangement produced the observed distribution. It is also possible that the changes in the bio-optical data were indicative of a temporal transition from *P. antarctica* to diatoms. This suggested temporal transition is in consonance with observations from both cell counts and accessory pigments (Ditullio et al., 2003; Peloquin and Smith, 2007; Smith et al., 2010).

4.2. Data resolution

The observed patterns and interpretation of water column properties from the glider observations would have been markedly different if they were sampled at lower resolution. To demonstrate this quantitatively, lower resolution station observations were obtained for comparison by subsampling casts from within the glider data set at a resolution (~50 km; Fig. 8) similar to that of traditional cruise stations (Smith and Asper, 2001; Hales and Takahashi, 2004). This subsampling was performed twice (Fig. 8a,c), and in both cases revealed patterns of temperature similar to those of the original, high-resolution data, but with a diminished extent of MCDW (Fig. 4a vs. 8a and c). In contrast, subsampled patterns of chlorophyll concentrations produce very different patterns (Fig. 5a vs. 8b and d). Shallow patches of elevated concentrations occur at opposite ends of the glider section depending on the particular set of stations selected (Fig. 8b,d). In addition, the mesoscale variability of temperature and chlorophyll through ~200 m that was observed from the full glider data set (Figs. 4a, and 5a) disappeared when these data were subsampled (Fig. 8). Instead, horizontal aliasing appeared in the visualization as a result of interpolating between distantly spaced data points. The surface diel fluorescence cycles likewise became obscured as a result of the subsampling.

Correlations between physical and biological variables in the subsampled sets also differed substantially from those computed from the full data set. The strongest correlations evident in the full data set between chlorophyll and SST and between POC and wind were insignificant after subsampling (Table 3). In contrast, the strongest correlates for chlorophyll and POC after subsampling were wind and MCDW thickness, respectively. Performing the subsampling twice with different station sets also produced different correlations, reflecting a strong dependence on specific station locations when assessing variable associations at lower resolutions. In addition, there were few significant correlations from the westward section, and all subsampled correlations within the eastward section were not significant. These diminished significances and dramatically altered correlations obtained after subsampling the glider data at cruise-station resolution demonstrate how high resolution data such as those described in this study offer important insights into biogeochemical variability that may be biased or obscured in lower resolution data sets.

5. Summary and conclusions

The glider observations described reveal environmental dynamics in the Southern Ross Sea at a level of resolution that are difficult to obtain by other means. Ship-based observations provide a lower resolution description of the multiple physical and biological transitions observed via glider, and the harsh conditions of the Ross Sea limit the feasibility of other high temporal resolution platforms. For example, moorings and their deployments are made challenging by ice, and frequent extensive cloud cover prohibits daily, unobstructed satellite imagery. This analysis of the distribution of high-resolution physical and bio-optical properties has demonstrated chlorophyll and POC trends consistent with a transition from a *P. antarctica*- to a diatom-dominated assemblage. Further, the depth of the mixed layer and MCDW were less associated with biological variations than SST and wind speed. Attributing causality and differentiating spatial and temporal effects is difficult when observing concurrent multivariate shifts, but glider-based approaches like ours can help. Further high-resolution surveys, and with additional sensors, will likely lead to a new and comprehensive picture of Ross Sea biogeochemical dynamics.

Acknowledgments

This material is based upon work supported by the U.S. National Science Foundation's Office of Polar Programs (NSF-ANT-0838980). The authors thank Drs. Craig Lee and Vernon Asper for technical assistance. Additional thanks go to Michael Dinniman, Yongjin Xiao, and Dylan O'Connell for their assistance at various stages of this research. The authors also acknowledge the constructive comments of Dr. Hein de Baar and two anonymous reviewers in the revision of the manuscript. This paper is Contribution No. 3370 of the Virginia Institute of Marine Science, College of William & Mary. The participation of BQ was supported by a bursary from Antarctic Science.

References

Alderkamp, A.-C., Kulk, G., Buma, A.G.J., Visser, R.J.W., van Dijken, G.L., Mills, M.M., Arrigo, K.R., 2012. The effect of iron limitation on the photophysiology of *Phaeocystis antarctica* (Prymnesiophyceae) and *Fragilariopsis cylindrus* (Bacillariophyceae) under dynamic irradiance. J. Phycol. 48, 45–59, http://dx.doi.org/10.1111/j.1529-8817.2011.01098.x.

Arrigo, K.R., Robinson, D.H., Worthen, D.L., Dunbar, R.B., DiTullio, G.R., VanWoert, M., Lizotte, M.P., 1999. Phytoplankton community structure and the drawdown of nutrients and CO_2 in the Southern Ocean. Science 283, 365–367, http://dx.doi.org/10.1126/science.283.5400.365.

Arrigo, K.R., Robinson, D.H., Worthen, D.L., Schieber, B., Lizotte, M.P., 1998. Bio-optical properties of the southwestern Ross Sea. J. Geophys. Res. 103, 21683–-21695, http://dx.doi.org/10.1029/98JC02157.

Arrigo, K.R., van Dijken, G., Long, M., 2008. Coastal Southern Ocean: a strong anthropogenic CO_2 sink. Geophys. Res. Lett. 35, 1–6, http://dx.doi.org/10.1029/2008GL035624.

Arrigo, K.R., Worthen, D., Robinson, D., 2003. A coupled ocean-ecosystem model of the Ross Sea: 2. Iron regulation of phytoplankton taxonomic variability and primary production. J. Geophys. Res., 108, http://dx.doi.org/10.1029/2001JC000856.

Behrenfeld, M.J., Worthington, K., Sherrell, R.M., Chavez, F.P., Strutton, P., McPhaden, M., Shea, D.M., 2006. Controls on tropical Pacific Ocean productivity revealed through nutrient stress diagnostics. Nature 442, 1025–1028, http://dx.doi.org/10.1038/nature05083.

Belcher, S.E., Grant, A.L.M., Hanley, K.E., Fox-Kemper, B., Van Roekel, L., Sullivan, P.P., Large, W.G., Brown, A., Hines, A., Calvert, D., Rutfersson, A., Pettersson, H., Bidlot, J-R., Janssen, P.A.E.M., Polton, J.A., 2012. A global perspective on Langmuir turbulence in the ocean surface boundary layer. Geophys. Res. Lett. 39, 1–9, http://dx.doi.org/10.1029/2012GL052932.

Boss, E., Pegau, W.S., 2001. Relationship of light scattering at an angle in the backward direction to the backscattering coefficient. Appl. Opt. 40, 5503–5507, http://dx.doi.org/10.1364/AO.40.005503.

Bracegirdle, T.J., Connolley, W.M., Turner, J., 2008. Antarctic climate change over the twenty first century. J. Geophys. Res. 113, 1–13, http://dx.doi.org/10.1029/2007JD008933.

Budillon, G., Pacciaroni, M., Cozzi, S., Rivaro, P., Catalano, G., Ianni, C., Cantoni, C., 2003. An optimum multiparameter mixing analysis of the shelf waters in the Ross Sea. Antarct. Sci. 15, 105–118, http://dx.doi.org/10.1017/S095410200300110X.

Buschmann, C., 1999. Photochemical and non-photochemical quenching coefficients of the chlorophyll fluorescence: comparison of variation and limits. Photosynthetica 37, 217–224, http://dx.doi.org/10.1023/A:1007003921135.

Caron, D.A., Dennett, M.R., Lonsdale, D.J., Moran, D.M., Shalapyonok, L., 2000. Microzooplankton herbivory in the Ross Sea, Antarctica. Deep-Sea Res. II 47, 3249–3272, http://dx.doi.org/10.1016/S0967-0645(00)00067-9.

Castro-Morales, K., Kaiser, J., 2012. Using dissolved oxygen concentrations to determine mixed layer depths in the Bellingshausen Sea. Ocean Sci. 8, 1–10, http://dx.doi.org/10.5194/osd-8-1505-2011.

Chu, P.C., Fan, C., 2011. Maximum angle method for determining mixed layer depth from seaglider data. J. Oceanogr. 67, 219–230, http://dx.doi.org/10.1007/s10872-011-0019-2.

De Boyer Montégut, C., Madec, G., Fischer, A.S., Lazar, A., Iudicone, D., 2004. Mixed layer depth over the global ocean: an examination of profile data and a profile-based climatology. J. Geophys. Res. 109, C12003, http://dx.doi.org/10.1029/2004JC002378.

Montégut, De Boyer, Mignot, C., Lazar, J., Cravatte, S., A., 2007. Control of salinity on the mixed layer depth in the world ocean: 1. General description. J. Geophys. Res. 112, C06011, http://dx.doi.org/10.1029/2006JC003953.
Dee, D.P., Uppala, S.M., Simmons, A.J., Berrisford, P., Poli, P., Kobayashi, S., Andrae, U., Balmaseda, M.A., Balsamo, G., Bauer, P., Bechtold, P., Beljaars, A.C.M., van de Berg, L., Bidlot, J., Bormann, N., Delsol, C., Dragani, R., Fuentes, M., Geer, A.J., Haimberger, L., Healy, S.B., Hersbach, H., Hólm, E.V., Isaksen, L., Kållberg, P., Köhler, M., Matricardi, M., McNally, A.P., Monge-Sanz, B.M., Morcrette, J.-J., Park, B.-K., Peubey, C., de Rosnay, P., Tavolato, C., Thépaut, J.-N., Vitart, F., 2011. The ERA-interim reanalysis: configuration and performance of the data assimilation system. Q. J. R. Meteorol. Soc. 137, 553–597, http://dx.doi.org/10.1002/qj.828.
Dennett, M.R., Mathot, S., Caron, D.A., Smith, W.O., Lonsdale, D.J., 2001. Abundance and distribution of phototrophic and heterotrophic nano- and microplankton in the southern Ross Sea. Deep-Sea Res. II 48, 4019–4037, http://dx.doi.org/10.1016/S0967-0645(01)00079-0.
Ditullio, G.R., Geesey, M.E., Leventer, A., Lizotte, M.P., 2003. Algal pigment ratios in the Ross Sea: implications for CHEMTAX analysis of Southern Ocean data. In: DiTullio, G.R., Dunbar, R. (Eds.), Biogeochemistry of the Ross Sea. Antarctic Research Series, vol. 78. American Geophysical Union, Washington DC http://dx.doi.org/10.1029/078ARS03.
DiTullio, G.R., Smith Jr., W.O., 1996. Spatial patterns in phytoplankton biomass and pigment distributions in the Ross Sea. J. Geophys. Res. 101, 18467–18477, http://dx.doi.org/10.1029/96JC00034.
Fragoso, G.M., Smith Jr., W.O., 2012. Influence of hydrography on phytoplankton distribution in the Amundsen and Ross Seas, Antarctica. J. Mar. Syst. 89, 19–29, http://dx.doi.org/10.1016/j.jmarsys.2011.07.008.
Fretwell, P., Pritchard, H.D., Vaughan, D.G., Bamber, J.L., Barrand, N.E., Bell, R., Bianchi, C., Bingham, R.G., Blankenship, D.D., Casassa, G., Catania, G., Callens, D., Conway, H., Cook, A.J., Corr, H.F.J., Damaske, D., Damm, V., Ferraccioli, F., Forsberg, R., Fujita, S., Gim, Y., Gogineni, P., Griggs, J.A., Hindmarsh, R.C.A., Holmlund, P., Holt, J.W., Jacobel, R.W., Jenkins, A., Jokat, W., Jordan, T., King, E.C., Kohler, J., Krabill, W., Riger-Kusk, M., Langley, K.A., Leitchenkov, G., Leuschen, C., Luyendyk, B.P., Matsuoka, K., Mouginot, J., Nitsche, F.O., Nogi, Y., Nost, O.A., Popov, S.V., Rignot, E., Rippin, D.M., Rivera, A., Roberts, J., Ross, N., Siegert, M.J., Smith, A.M., Steinhage, D., Studinger, M., Sun, B., Tinto, B.K., Welch, B.C., Wilson, D., Young, D.A., Xiangbin, C., Zirizzotti, A., 2013. Bedmap2: improved ice bed, surface and thickness datasets for Antarctica. Cryosphere 7, 375–393, http://dx.doi.org/10.5194/tc-7-375-2013.
Friedrichs, M.A.M., Hofmann, E.E., 2001. Physical control of biological processes in the central equatorial Pacific Ocean. Deep-Sea Res. I 48, 1023–1069, http://dx.doi.org/10.1016/S0967-0637(00)00079-0.
Garau, B., Ruiz, S., Zhang, W.G., Pascual, A., Heslop, E., Kerfoot, J., Tintoré, J., 2011. Thermal lag correction on Slocum CTD glider data. J. Atmos. Ocean. Technol. 28, 1065–1071, http://dx.doi.org/10.1175/JTECH-D-10-05030.1.
Gardner, W.D., Richardson, M.J., Smith Jr., W.O., 2000. Seasonal patterns of water column particulate organic carbon and fluxes in the Ross Sea, Antarctica. Deep-Sea Res. II 47, 3423–3449, http://dx.doi.org/10.1016/S0967-0645(00)00074-6.
Hales, B., Takahashi, T., 2004. High-resolution biogeochemical investigation of the Ross Sea, Antarctica, during the AESOPS (U. S. JGOFS) program. Glob. Biogeochem. Cycles 18, 1–24, http://dx.doi.org/10.1029/2003GB002165.
Heinemann, G., Klein, T., 2003. Simulations of topographically forced mesocyclones in the Weddell Sea and the Ross Sea region of Antarctica. Mon. Weather Rev. 131, 302–316, http://dx.doi.org/10.1175/1520-0493(2003)131<0302:SOTFMI>2.0.CO;2.
Heywood, K.J., Schmidtko, S., Heuzé, C., Kaiser, J., Jickells, T.D., Queste, B.Y., Stevens, D.P., Wadley, M., Thompson, A.F., Fielding, S., Guihen, D., Creed, E., Ridley, J.K., Smith, W., 2014. Ocean processes at the Antarctic continental slope. Philos. Trans. R. Soc. A Math. Phys. Eng. Sci 372, 1–11, http://dx.doi.org/10.1098/rsta.2013.0047.
Hiscock, M.R., 2004. The regulation of primary productivity in the Southern Ocean (Ph.D. dissertation). Duke University p. 150.
Holte, J., Talley, L., 2009. A new algorithm for finding mixed layer depths with applications to Argo data and subantarctic mode water formation. J. Atmos. Ocean. Technol. 26, 1920–1939, http://dx.doi.org/10.1175/2009JTECHO543.1.
Jacobs, S.S., Giulivi, C.F., 2010. Large multidecadal salinity trends near the Pacific–Antarctic continental margin. J. Clim. 23, 4508–4524, http://dx.doi.org/10.1175/2010JCLI3284.1.
Jacobs, S.S., Giulivi, C., Mele, P.A., 2002. Freshening of the Ross Sea during the late 20th century. Science 297, 386–389, http://dx.doi.org/10.1126/science.1069574.
Jackett, D.R., McDougall, T.J., 1997. A neutral density variable for the world's oceans. J. Phys. Oceanogr. 27, 237–263, http://dx.doi.org/10.1175/1520-0485(1997)027<0237:ANDVFT>2.0.CO;2.
Kalnay, E., Kanamitsu, M., Kistler, R., Collins, W., Deaven, D., Gandin, L., Iredell, M., Saha, S., White, G., Woollen, J., Zhu, Y., Chelliah, M., Ebisuzaki, W., Higgins, W., Janowiak, J., Mo, K.C., Ropelewski, C., Wang, J., Leetmaa, A., Reynolds, R., Jenne, R., Joseph, D., 1996. The NCEP/NCAR 40-year reanalysis project. Bull. Am. Meteorol. Soc. 77, 437–471, http://dx.doi.org/10.1175/1520-0477(1996)077<0437:TNYRP>2.0.CO;2.
Kohut, J., Hunter, E., Huber, B., 2013. Small-scale variability of the cross-shelf flow over the outer shelf of the Ross Sea. J. Geophys. Res. Ocean 118, 1863–1876, http://dx.doi.org/10.1002/jgrc.20090.
Kropuenske, L.R., Mills, M.M., van Dijken, G.L., Bailey, S., Robinson, D.H., Welschmeyer, N.A., Arrigo, K.R., 2009. Photophysiology in two major southern ocean phytoplankton taxa: photoprotection in *Phaeocystis antarctica* and *Fragilariopsis cylindrus*. Limnol. Oceanogr. 54, 1176–1196, http://dx.doi.org/10.1093/icb/icq021.
Liu, X., Smith Jr., W.O., 2012. Physiochemical controls on phytoplankton distributions in the Ross Sea, Antarctica. J. Mar. Syst. 94, 135–144, http://dx.doi.org/10.1016/j.jmarsys.2011.11.013.
Long, M.C., Thomas, L.N., Dunbar, R.B., 2012. Control of phytoplankton bloom inception in the Ross Sea, Antarctica, by Ekman restratification. Glob. Biogeochem. Cycles 26, 1–14, http://dx.doi.org/10.1029/2010GB003982.
Lueck, R.G., Picklo, J.J., 1990. Thermal inertia of conductivity cells: observations with a Sea-Bird cell. J. Atmos. Ocean. Technol. 7, 756–768, http://dx.doi.org/10.1175/1520-0426(1990)007<0756:TIOCCO>2.0.CO;2.
Mahadevan, A., D'Asaro, E., Lee, C., Perry, M.J., 2012. Eddy-driven stratification initiates North Atlantic spring phytoplankton blooms. Science 337, 54–58, http://dx.doi.org/10.1126/science.1218740.
Massom, R.A., Stammerjohn, S.E., 2010. Antarctic sea ice change and variability – physical and ecological implications. Polar Sci 4, 149–186, http://dx.doi.org/10.1016/j.polar.2010.05.001.
Mathot, S., Smith Jr., W.O., Carlson, C.A., Garrison, D.L., Gowing, M.M., Vickers, C.L., 2000. Carbon partitioning within *Phaeocystis antarctica* (*Prymnesiophyceae*) colonies in the Ross Sea, Antarctica. J. Phycol. 36, 1049–1056, http://dx.doi.org/10.1046/j.1529-8817.2000.99078.x.
McGillicuddy Jr., D.J., Anderson, L.A., Bates, N.R., Bibby, T., Buesseler, K.O., Carlson, C.A., Davis, C.S., Ewart, C., Falkowski, P.G., Goldthwait, S.A., Hansell, D.A., Jenkins, W.J., Johnson, R., Kosnyrev, V.K., Ledwell, J.R., Li, Q.P., Siegel, D.A., Steinberg, D.K., 2007. Eddy/wind interactions stimulate extraordinary mid-ocean plankton blooms. Science 316, 1021–1026, http://dx.doi.org/10.1126/science.1136256.
Morel, A., 1974. Optical properties of pure water and pure sea water. In: Jerlov, N.G., Steemann-Nielsen, E. (Eds.), Optical Aspects of Oceanography. Academic Press, London, pp. 1–24.
Morison, J., Andersen, R., Larson, N., D'Asaro, E., Boyd, T., 1994. The correction for thermal-lag effects in Sea-Bird CTD data. J. Atmos. Ocean. Technol. 11, 1151–1164, http://dx.doi.org/10.1175/1520-0426(1994)011<1151:TCFTLE>2.0.CO;2.
Orsi, A.H., Wiederwohl, C.L., 2009. A recount of Ross Sea waters. Deep-Sea Res. II 56, 778–795, http://dx.doi.org/10.1016/j.dsr2.2008.10.033.
Peloquin, J.A., Smith Jr., W.O., 2007. Phytoplankton blooms in the Ross Sea, Antarctica: Interannual variability in magnitude, temporal patterns, and composition. J. Geophys. Res. 112, 1–12, http://dx.doi.org/10.1029/2006JC003816.
Queste B.Y., Hydrographic observations of oxygen and related physical variables in the North Sea and Western Ross Sea Polynya. Investigations using Seagliders, historical observations and numerical modeling. PhD Thesis, University of East Anglia, UK, 2014.
Robertson, R., 2005. Baroclinic and barotropic tides in the Ross Sea. Antarct. Sci. 17, 107–120, http://dx.doi.org/10.1017/S0954102005002506.
Saba, V.S., Friedrichs, M.A.M., Antoine, D., Armstrong, R.A., Asanuma, I., Behrenfeld, M.J., Ciotti, A.M., Dowell, M., Hoepffner, N., Hyde, K.J.W., Ishizaka, J., Kameda, T., Marra, J., Mélin, F., Morel, A., O'Reilly, J., Scardi, M., Smith, W.O., Smyth, T.J., Tang, S., Uitz, J., Waters, K., Westberry, T.K., 2011. An evaluation of ocean color model estimates of marine primary productivity in coastal and pelagic regions across the globe. Biogeosciences 8, 489–503, http://dx.doi.org/10.5194/bg-8-489-2011.
Schoemann, V., Becquevort, S., Stefels, J., Rousseau, V., Lancelot, C., 2005. Phaeocystis blooms in the global ocean and their controlling mechanisms: a review. J. Sea Res. 53, 43–66, http://dx.doi.org/10.1016/j.seares.2004.01.008.
Sedwick, P.N., Marsay, C.M., Sohst, B.M., Aguilar-Islas, A.M., Lohan, M.C., Long, M.C., Arrigo, K.R., Dunbar, R.B., Saito, M.A., Smith Jr., W.O., DiTullio, G.R., 2011. Early season depletion of dissolved iron in the Ross Sea polynya: implications for iron dynamics on the Antarctic continental shelf. J. Geophys. Res. 116, C12019, http://dx.doi.org/10.1029/2010JC006553.
Smith Jr., W.O., Asper, V.L., 2001. The influence of phytoplankton assemblage composition on biogeochemical characteristics and cycles in the southern Ross Sea, Antarctica. Deep-Sea Res. I 48, 137–161.
Smith Jr., W.O., Asper, V., Tozzi, S., Liu, X., Stammerjohn, S.E., 2011a. Surface layer variability in the Ross Sea, Antarctica as assessed by in situ fluorescence measurements. Prog. Oceanogr 88, 28–45, http://dx.doi.org/10.1016/j.pocean.2010.08.002.
Smith Jr., W.O., Carlson, C.A., Ducklow, H.W., Hansell, D.A., 1998. Growth dynamics of *Phaeocystis antarctica*-dominated plankton assemblages from the Ross Sea. Mar. Ecol. Prog. Ser. 168, 229–244, http://dx.doi.org/10.3354/meps168229.
Smith Jr., W.O., Comiso, J.C., 2008. Influence of sea ice on primary production in the Southern Ocean: a satellite perspective. J. Geophys. Res. 113, 1–19, http://dx.doi.org/10.1029/2007JC004251.
Smith Jr., W.O., Dennett, M.R., Mathot, S., Caron, D.A., 2003. The temporal dynamics of the flagellated and colonial stages of *Phaeocystis antarctica* in the Ross Sea. Deep-Sea Res. II 50, 605–617, http://dx.doi.org/10.1016/S0967-0645(02)00586-6.
Smith Jr., W.O., Dinniman, M.S., Tozzi, S., DiTullio, G.R., Mangoni, O., Modigh, M., Saggiomo, V., 2010. Phytoplankton photosynthetic pigments in the Ross Sea: patterns and relationships among functional groups. J. Mar. Syst. 82, 177–185, http://dx.doi.org/10.1016/j.jmarsys.2010.04.014.
Smith Jr., W.O., Goetz, K.T., Kaufman, D.E., Queste, B.Y., Asper, V., Costa, D.P., Dinniman, M.S., Friedrichs, M.A.M., Hofmann, E.E., Heywood, K.J., Klinck, J.M., Kohut, J.T., Lee, C.M., 2014. Multiplatform, multidisciplinary investigations of the impacts of Modified Circumpolar Deep Water in the Ross Sea, Antarctica. Oceanography 27 (2), 180–185, http://dx.doi.org/10.5670/oceanog.2014.36.
Smith Jr., W.O., Gordon, L.I., 1997. Hyperproductivity of the Ross Sea (Antarctica) polynya during austral spring. Geophys. Res. Lett. 24, 233–236, http://dx.doi.org/10.1029/96GL03926.
Smith Jr., W.O., Marra, J., Hiscock, M.R., Barber, R.T., 2000. The seasonal cycle of phytoplankton biomass and primary productivity in the Ross Sea, Antarctica. Deep-Sea Res. I 47, 3119–3140, http://dx.doi.org/10.1016/S0967-0645(00)00061-8.
Smith Jr., W.O., Shields, A.R., Dreyer, J.C., Peloquin, J.A., Asper, V.L., 2011b. Interannual variability in vertical export in the Ross Sea: magnitude, composition, and environmental correlates. Deep-Sea Res. I 58, 147–159, http://dx.doi.org/10.1016/j.dsr.2010.11.007.

Sokal, R.R., Rohlf, F.J., 1969. Biometry. W.H. Freeman and Co., San Francisco (776 pp).

Stammerjohn, S., Massom, R., Rind, D., Martinson, D., 2012. Regions of rapid sea ice change: an inter-hemispheric seasonal comparison. Geophys. Res. Lett. 39, L06501, http://dx.doi.org/10.1029/2012GL050874.

Strzepek, R.F., Hunter, K.A., Frew, R.D., Harrison, P.J., Boyd, P.W., 2012. Iron–light interactions differ in Southern Ocean phytoplankton. Limnol. Oceanogr. 57, 1182–1200, http://dx.doi.org/10.4319/lo.2012.57.4.1182.

Tagliabue, A., Arrigo, K.R., 2003. Anomalously low zooplankton abundance in the Ross Sea: an alternative explanation. Limnol. Oceanogr. 48, 686–699, http://dx.doi.org/10.4319/lo.2003.48.2.0686.

Van de Poll, W., Lagunas, M., de Vries, T., Visser, R.J.W., Buma, A.G.J., 2011. Non-photochemical quenching of chlorophyll fluorescence and xanthophyll cycle responses after excess PAR and UVR in *Chaetoceros brevis*, *Phaeocystis antarctica* and coastal Antarctic phytoplankton. Mar. Ecol. Prog. Ser. 426, 119–131, http://dx.doi.org/10.3354/meps09000.